

Dynamical Mean-Field Theory of Complex Systems on Sparse Directed Networks

Fernando L. Metz

Physics Institute, Federal University of Rio Grande do Sul, 91501-970 Porto Alegre, Brazil

(Dated: June 11, 2024)

Although real-world complex systems typically interact through sparse and heterogeneous networks, analytic solutions of their dynamics are limited to models with all-to-all interactions. Here, we solve the dynamics of a broad range of nonlinear models of complex systems on sparse directed networks with a random structure. By generalizing dynamical mean-field theory to sparse systems, we derive an exact equation for the path-probability describing the effective dynamics of a single degree of freedom. Our general solution applies to key models in the study of neural networks, ecosystems, epidemic spreading, and synchronization. Using the population dynamics algorithm, we solve the path-probability equation to determine the phase diagram of a seminal neural network model in the sparse regime, showing that this model undergoes a transition from a fixed-point phase to chaos as a function of the network topology.

Introduction. Complex dynamical systems are modeled by N degrees of freedom $x_i(t)$ ($i = 1, \dots, N$) that evolve in time according to the coupled differential equations

$$\dot{x}_i(t) = -f(x_i) + \sum_{j=1}^N A_{ij}g(x_i, x_j) + \xi_i(t), \quad (1)$$

where $\{A_{ij}\}_{i,j=1,\dots,N}$ defines the interaction network and $\xi_i(t)$ is an uncorrelated Gaussian noise, with mean zero and variance σ^2 . The variable $\xi_i(t)$ models external random perturbations, the function $f(x)$ governs the dynamics in the absence of interactions, and the kernel $g(x, x')$ shapes the pairwise couplings. Equation (1) models the nonequilibrium dynamics of neural networks [1–5] and ecosystems [6–8], epidemic spreading [9–12], synchronization phenomena [13–15], opinion dynamics [16, 17], and multivariate Ornstein-Uhlenbeck processes [18–20]. Table I specifies $f(x)$ and $g(x, x')$ for paradigmatic models of complex behavior.

Model	$f(x)$	$g(x, x')$
Ornstein-Uhlenbeck (OU) process [18]	x	x'
SIS model of epidemic spreading [9]	x	$(1-x)x'$
Lotka-Volterra (LV) model [7, 8]	$x(x-1)$	xx'
Neural network (NN) model [1, 4]	x	$\tanh(x')$
Kuramoto model [14]	0	$\sin(x'-x)$

TABLE I. Explicit form of $f(x)$ and $g(x, x')$ in complex systems modeled by Eq. (1).

The foremost problem in the study of complex systems is how to reduce the dynamics of many interacting elements to the dynamics of a few variables [21]. Dynamical mean-field theory (DMFT) [22–24] is a powerful method to tackle this problem in the limit $N \rightarrow \infty$, yielding a solution in terms of the path-probability for the effective dynamics of a single degree of freedom. The application of DMFT to models described by Eq. (1) has been attracting an enormous interest [2–5, 7, 8, 15, 19, 20, 25–31], especially in the context of neural networks and

ecosystems. Phase diagrams of these models reveal a rich phenomenology, including different types of phase transitions [5, 7], chaotic behavior [1, 3], and coexistence of multiple attractors [7, 8, 32]. Despite this substantial theoretical progress, DMFT is currently limited to fully-connected networks, where each dynamical variable is coupled to *all* others by means of Gaussian interaction strengths. Nevertheless, the interactions in real-world complex systems are known to be *sparse* and *heterogeneous* [33, 34]. Sparseness indicates that each element of the system interacts on average with a finite number of others, while heterogeneity refers to fluctuations in the local topology of the interaction network. How to integrate these features in the formalism of DMFT for systems modeled by Eq. (1) remains an unresolved challenge, and even basic questions, such as characterizing the phase diagram of sparse complex systems, are still out of reach.

On the other hand, the dynamics of complex systems on sparse networks has been extensively studied in the case of Ising spins [35–44]. In this context, both the cavity method [36] and DMFT [35, 37] provide an analytic solution in terms of the path-probability for the effective dynamics of a single unit. However, the presence of symmetric interactions induce a temporal feedback, which, in the particular case of sparse systems, leads to an exponential growth of the path-probability dimension [35, 37, 43], rendering numerical computations unfeasible. When the interactions are directed or unidirectional, this issue does not arise, allowing the path-probability equation to be efficiently solved [35, 36, 45].

Inspired by these results for Ising spins, in this letter we solve the dynamics of models governed by Eq. (1) on sparse directed networks with an heterogeneous topology. The solution represents a foundational step in the study of sparse complex systems, as it ultimately incorporates the role of the network structure in the formalism of DMFT. Besides that, directed networks are interesting from a practical viewpoint, because they model the non-reciprocal interactions in real-world complex sys-

tems [46], including the synaptic connections in the human cortex [47] and the trophic interactions in food-webs [34, 48, 49].

By generalizing DMFT to sparse systems, we obtain an exact equation for the path-probability describing the effective dynamics of a single variable for $N \rightarrow \infty$. We solve this equation for different models in table I by using the population dynamics algorithm [50, 51], which is a fundamental tool in the study of sparse disordered systems [52–55]. The excellent agreement between our theoretical results and numerical simulations of finite systems confirms that our solution is valid for several models.

As an application, we determine the phase diagram of the neural network model by Sompolinsky *et al* [1] in the sparse regime. We show that the phase diagram displays a trivial fixed-point phase, a nontrivial fixed-point phase, and a chaotic region. Our results for the transition lines, based on the dynamics of macroscopic observables, are consistent with the universal critical lines derived from random matrix theory [56–58]. Remarkably, we provide evidence that the transition from the nontrivial fixed-point phase to the chaotic regime coincides with the vanishing of the gap between the leading eigenvalue and the bulk of the network spectrum.

Sparse directed networks. Let $A_{ij} = C_{ij}J_{ij}$ be the elements of the $N \times N$ interaction matrix \mathbf{A} . The binary variables $C_{ij} \in \{0, 1\}$ determine the network topology, while $J_{ij} \in \mathbb{R}$ controls the pairwise interaction strengths. If $C_{ij} = 1$, there is a directed edge $j \rightarrow i$ pointing from node j to i , while $C_{ij} = 0$ otherwise. We also set $C_{ii} = 0$. The indegree $K_i = \sum_{j=1}^N C_{ij}$ and the outdegree $L_i = \sum_{j=1}^N C_{ji}$ count the number of links entering and leaving node i [33], respectively. The random variables $\{C_{ij}\}_{i \neq j}$ follow the distribution

$$\mathbb{P}(\{C_{ij}\}) = \frac{1}{\mathcal{N}} \prod_{i \neq j=1}^N \left[\frac{c}{N} \delta_{C_{ij},1} + \left(1 - \frac{c}{N}\right) \delta_{C_{ij},0} \right] \times \prod_{i=1}^N \delta_{K_i, \sum_{j=1}^N C_{ij}} \delta_{L_i, \sum_{j=1}^N C_{ji}}, \quad (2)$$

where \mathcal{N} is the normalization constant. The degrees $\{K_i, L_i\}_{i=1, \dots, N}$ are independent and identically distributed random variables drawn from $p_{k,\ell} = p_{\text{in},k} p_{\text{out},\ell}$, where $p_{\text{in},k}$ and $p_{\text{out},\ell}$ are the indegree and the outdegree distribution [33, 53], respectively. The network parameter c is the average degree

$$c = \sum_{k=0}^{\infty} k p_{\text{in},k} = \sum_{\ell=0}^{\infty} \ell p_{\text{out},\ell}. \quad (3)$$

Equation (2) defines a network ensemble where directed links are randomly placed between pairs of nodes with probability c/N , subject to the prescribed degree sequences generated from $p_{k,\ell}$. In the limit $N \rightarrow \infty$, the network samples generated from Eq. (2) are equivalent

to those produced by the configuration model [59, 60]. The coupling strengths $\{J_{ij}\}_{i,j=1, \dots, N}$ are independent and identically distributed random variables drawn from a distribution p_J with mean μ_J and variance σ_J^2 . The distributions $p_{k,\ell}$ and p_J fully specify the network ensemble, allowing for a systematic investigation of how network heterogeneities impact the dynamics of complex systems.

Solution through DMFT. We solve the coupled dynamics of Eq. (1) on directed networks by using dynamical mean-field theory (DMFT) [22–24]. We consider the sparse regime, where the mean degree c is *finite*, independent of N . DMFT is based on the generating functional

$$\mathcal{Z}[\boldsymbol{\psi}] = \int \left(\prod_{i=1}^N Dx_i \right) \mathcal{P}[\mathbf{x}] e^{i \int dt \sum_{i=1}^N x_i(t) \psi_i(t)} \quad (4)$$

of the probability density $\mathcal{P}[\mathbf{x}]$ of observing a dynamical path of states $\mathbf{x}(t) = (x_1(t), \dots, x_N(t))$ in a fixed time interval. The correlation functions of $\{x_i(t)\}_{i=1, \dots, N}$ follow from the derivatives of $\mathcal{Z}[\boldsymbol{\psi}]$ with respect to the external sources $\boldsymbol{\psi}(t) = (\psi_1(t), \dots, \psi_N(t))$. In particular, the n th-moment of the local variable $x_i(t)$,

$$\langle x_i^n(t) \rangle = \int \left(\prod_{i=1}^N Dx_i \right) x_i^n(t) \mathcal{P}[\mathbf{x}] = (-i)^n \left. \frac{\delta^n \mathcal{Z}[\boldsymbol{\psi}]}{\delta \psi_i^n(t)} \right|_{\boldsymbol{\psi}=0}, \quad (5)$$

yields the time-evolution of the macroscopic quantities

$$m(t) = \lim_{N \rightarrow \infty} \frac{1}{N} \sum_{i=1}^N \langle x_i(t) \rangle, \quad q(t) = \lim_{N \rightarrow \infty} \frac{1}{N} \sum_{i=1}^N \langle x_i^2(t) \rangle. \quad (6)$$

Clearly, the generating functional fulfills $\mathcal{Z}[0] = 1$.

In the supplemental material [61], we calculate the average of $\mathcal{Z}[\boldsymbol{\psi}]$ over the network ensemble defined by Eq. (2) for finite c , recasting the problem in terms of the solution of a saddle-point integral. More importantly, we give a clear physical interpretation of the order-parameters, simplifying the saddle-point equations and obtaining a feasible solution for the dynamics in the sparse regime. In the limit $N \rightarrow \infty$, the microscopic dynamical variables decouple, and the path-probability $\mathcal{P}[x]$ for the effective dynamics of a single variable $x(t)$ is determined from

$$\mathcal{P}[x] = \sum_{k=0}^{\infty} p_{\text{in},k} \int \left(\prod_{j=1}^k Dx_j \mathcal{P}[x_j] \right) \int \left(\prod_{j=1}^k dJ_j p_J(J_j) \right) \times \left\langle \delta_F \left[\dot{x}(t) + f(x(t)) - \sum_{j=1}^k J_j g(x(t), x_j(t)) - \xi(t) \right] \right\rangle_{\xi} \quad (7)$$

where δ_F is the functional Dirac- δ , and $\langle \dots \rangle_{\xi}$ represents the average over the uncorrelated Gaussian noise $\xi(t)$. The macroscopic observables are given by $m(t) = \langle x(t) \rangle_*$

and $q(t) = \langle x^2(t) \rangle_*$, where

$$\langle x^n(t) \rangle_* = \int Dx x^n(t) \mathcal{P}[x] \quad (n = 1, 2) \quad (8)$$

is the average over the effective dynamics governed by $\mathcal{P}[x]$. The self-consistent Eq. (7) is the exact solution of a broad class of models (see table I) on sparse directed networks with arbitrary distributions p_J and $p_{k,\ell} = p_{\text{in},k} p_{\text{out},\ell}$. We solve the more general case of networks with correlated indegrees and outdegrees in [61]. The solution of Eq. (7) determines the time-evolution of the full probability distribution of the microscopic variables in the limit $N \rightarrow \infty$.

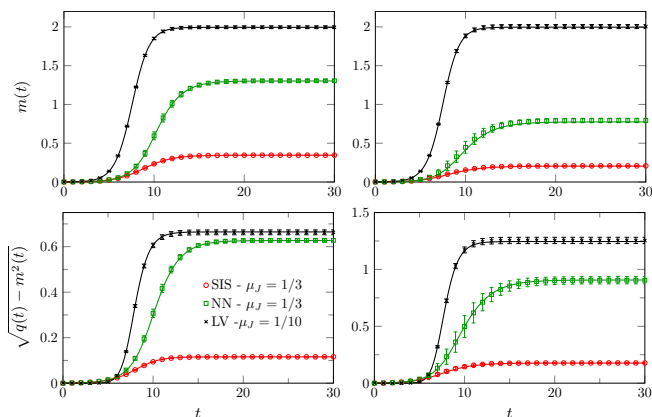


FIG. 1. Dynamics of the mean $m(t)$ and the standard deviation $\sqrt{q(t) - m^2(t)}$ for the SIS model, LV model, and NN model (see table I) without external noise ($\sigma = 0$). Results are shown for directed random networks with average degree $c = 5$ and two indegree distributions (Eq. (9)): Poisson (left column) and geometric (right column). The distribution p_J of the coupling strengths has mean μ_J and standard deviation $\sigma_J = 0.1$. For the LV and NN models, p_J is Gaussian; for the SIS model, p_J is uniform. Solid lines are solutions of Eq. (7) using the population dynamics algorithm with 5×10^4 paths. Symbols denote numerical simulations of Eq. (1) for an ensemble of 10 independent random networks generated from the configuration model with $N = 4000$ nodes. Vertical bars are the standard deviation of the macroscopic observables.

From now on, we set $\sigma = 0$ in Eq. (7) and study the dynamics in the absence of external noise. Below we present results for Poisson and geometric indegrees, where the indegree distribution $p_{\text{in},k}$ is given by

$$p_{\text{in},k} = \frac{c^k e^{-c}}{k!} \quad \text{and} \quad p_{\text{in},k} = \frac{c^k}{(c+1)^{k+1}}, \quad (9)$$

respectively.

Equation (7) is formally similar to other distributional equations appearing in the study of sparse disordered systems [50–55]. Therefore, we can numerically solve this equation using the population dynamics algorithm [50, 52, 53]. In the standard version of this algorithm

[50, 53], a probability density is parametrized by a population of stochastic variables. Here, we generalize the algorithm to calculate $\mathcal{P}[x]$ by introducing a population of dynamical trajectories. At each iteration step, a single path is chosen randomly from the population and updated according to the differential equation imposed by the Dirac- δ_F in Eq. (7). After sufficient iterations, the population of paths converges to a stationary distribution, providing a numerical solution for $\mathcal{P}[x]$. A detailed account of the algorithm is in [61].

In Fig. 1, we compare the solutions of Eq. (7) with numerical simulations of the original coupled dynamics, Eq. (1), for finite N . The panels showcase the time-evolution of the mean $m(t)$ and the standard deviation $\sqrt{q(t) - m^2(t)}$ of the microscopic variables for different network topologies and three important models of complex systems (see table I): the NN model of [1], the LV model, and the SIS model of epidemic spreading. In all cases, the agreement between our theoretical results for $N \rightarrow \infty$ and numerical simulations for large N is excellent, confirming the exactness of Eq. (7).

An important question is whether Eq. (7) recovers the analytic results of fully-connected models as $c \rightarrow \infty$ [1, 4, 26]. We show in [61] that this is generally not the case. In the high-connectivity limit $c \rightarrow \infty$, degree fluctuations remain significant, and $\mathcal{P}[x]$ depends on the full distribution $\nu_{\text{in}}(\kappa)$ of rescaled indegrees $\kappa_i = K_i/c$ ($i = 1, \dots, N$). The well-known effective dynamics on fully-connected networks is only recovered when $\nu_{\text{in}}(\kappa) = \delta(\kappa - 1)$. This breakdown in the universality of fully-connected models due to degree fluctuations was anticipated in [62–65].

Phase diagram of neural networks. Now we derive the phase diagram of the NN model on sparse directed networks for $\sigma = 0$. In this context, $x_i(t) \in \mathbb{R}$ represents the synaptic current at neuron i , $f(x) = x$, and $g(x, x') = \tanh(x')$. Let us order the complex eigenvalues $\{\lambda_\alpha\}_{\alpha=1, \dots, N}$ of \mathbf{A} according to their real parts as $\text{Re}\lambda_1 > \text{Re}\lambda_2 > \dots > \text{Re}\lambda_N$. A linear stability analysis of Eq. (1) shows that $\mathbf{x} = 0$ is stable if $\text{Re}\lambda_1 < 1$. Based on previous analytic results for the spectra of directed networks for $N \rightarrow \infty$ [56–58], we find that the trivial fixed-point is stable provided $c < c_{\text{stab}}$, where

$$c_{\text{stab}} = \begin{cases} 1/\mu_J & \text{if } c > 1 + \sigma_J^2/\mu_J^2, \\ 1/(\sigma_J^2 + \mu_J^2) & \text{if } c \leq 1 + \sigma_J^2/\mu_J^2. \end{cases} \quad (10)$$

The two distinct regimes in Eq. (10) result from the gap-gapless transition in the spectrum of \mathbf{A} [56]. For $c > 1 + \sigma_J^2/\mu_J^2$, the spectral gap $|\lambda_1 - \lambda_2|$ remains finite as $N \rightarrow \infty$, while it vanishes for $c \leq 1 + \sigma_J^2/\mu_J^2$. Equation (10) holds for $\mu_J > 0$ and $c > 1$. The later condition ensures that directed random networks contain a giant strongly connected component [66].

We emphasize that the above stability analysis does not give insights into the model’s dynamical behavior.

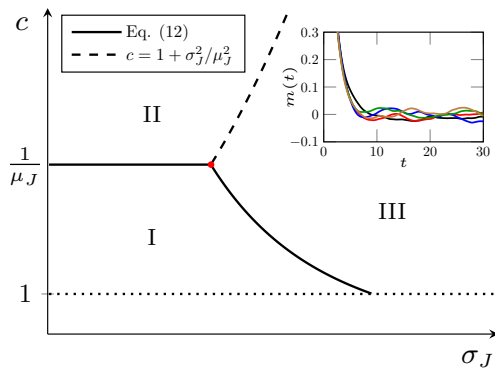


FIG. 2. Phase diagram (c, σ_J) of the NN model for fixed $0 < \mu_J < 1$. The macroscopic variables $m(t)$ and $q(t)$ relax to trivial and nontrivial fixed-points in phases I and II, respectively. In the chaotic phase III, $m(t)$ shows aperiodic oscillations around zero. The dotted line at $c = 1$ marks the percolation threshold, while the dashed curve identifies the gap-gapless transition (see the main text). The inset illustrates the sensitivity of $m(t)$ to small perturbations in the initial conditions. Each colored curve represents the numerical solution of Eq. (7) using population dynamics with 5×10^5 paths, with initial states sampled from a uniform distribution with unit mean and standard deviation of $\mathcal{O}(10^{-5})$. The red dot is located at $(c^*, \sigma_J^*) = (\mu_J^{-1}, \sqrt{\mu_J(1 - \mu_J)})$.

Therefore, we study the dynamics of $m(t)$ and $q(t)$ by solving Eq. (7). Figure 2 presents the resulting phase diagram. In phase I, $m(t)$ and $q(t)$ relax exponentially to the trivial solution $m = q = 0$, while in phase II, $m(t)$ and $q(t)$ evolve to nonzero fixed-points. In phase III, the neural network exhibits chaotic behavior, characterized by slow and aperiodic oscillations of $m(t)$ around zero. The inset in Fig. 2 illustrates the sensitivity of $m(t)$ to small perturbations in the initial conditions, a hallmark of deterministic chaos [67]. In phase III, the distribution of neural firing rates $\tanh(x_i(t))$ does not evolve to a stationary profile. The phase diagram in Fig. 2 is universal, as the transition lines depend only on the first and second moments of p_J and $p_{in,k}$.

Figure 3 characterizes the transition between phases I and II. As c approaches the critical mean degree $c^* = \mu_J^{-1}$ from above, the nontrivial fixed-point $m = m(t)$ vanishes continuously. The critical point c^* is independent of $p_{in,k}$, as predicted by Eq. (10), and $m(t)$ relaxes exponentially fast inside phases I and II. Due to critical slowing down, the numerical solution of Eq. (7) becomes computationally more demanding near c^* . In phase II, the neuronal firing rates evolve to a stationary distribution with a finite variance.

Figure 4 shows the dynamics of $m(t)$ and $q(t)$ across the transition between the fixed-point phases and the chaotic regime. Since $m(t)$ remains close to zero in both phases I and III, this is not an effective parameter to probe the transition between them. The second mo-

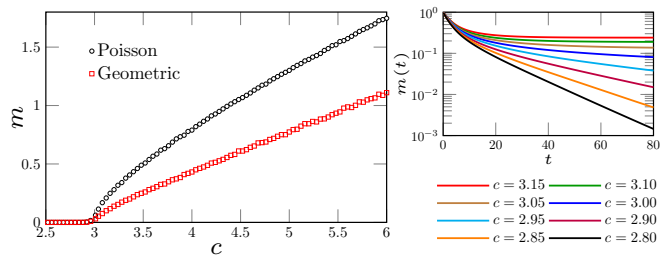


FIG. 3. Continuous transition between the fixed-point phases for the NN model on directed random networks. The coupling strengths follow a Gaussian distribution with mean $\mu_J = 1/3$ and standard deviation $\sigma_J = 0.1$. The results are derived from Eq. (7) using population dynamics with 5×10^5 paths. (a) Fixed-point solution $m(t) = m$ as a function of c for Poisson and geometric indegrees (Eq. (9)). (b) Dynamics of $m(t)$ across the transition for Poisson indegrees.

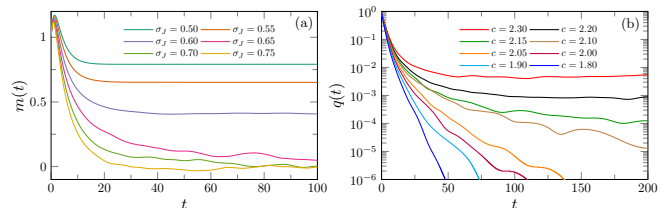


FIG. 4. Dynamics of $m(t)$ and $q(t)$ for the NN model on directed random networks with Poisson indegrees. Random coupling strengths follow a Gaussian distribution with mean $\mu_J = 1/3$ and standard deviation σ_J . The results are derived from the solutions of Eq. (7) using population dynamics with 5×10^5 paths. (a) Transition between phases II and III for $c = 5$. The critical value of σ_J is consistent with the dashed line in Fig. 2. (b) Transition between phases I and III for $\sigma_J = 0.6$. The critical value of c is consistent with Eq. (10).

ment $q(t)$, instead, clearly identifies the transition between phases I and III, as seen in Fig. 4(b). In this respect, this is analogous to the transition between the paramagnetic and the spin-glass phase [5, 68]. The critical line between phases II and III is not determined by the above stability analysis. Figure 4(a) illustrates the dynamics of $m(t)$ as the variance σ_J^2 of the couplings increases. Notably, the value of σ_J marking the sudden drop of $m(t)$ and the onset of chaotic oscillations is consistent with the dashed line in Fig. 2 (see [61] for additional results). This strongly suggests that the transition between phases II and III is governed by the gap $|\lambda_1 - \lambda_2|$ in the spectrum of directed random networks.

Conclusions. We have developed a dynamical mean-field theory of complex systems on sparse directed networks, deriving an exact path-probability equation for the effective dynamics in the limit $N \rightarrow \infty$. Unlike sparse models with symmetric interactions [35, 36], our path-probability equation can be numerically solved us-

ing population dynamics [53]. We confirmed the exactness of our general solution by comparing it with numerical simulations of fundamental models in the study of epidemic spreading, neural networks, and ecosystems. Finally, we applied our solution to determine the complete phase diagram of the sparse and directed version of the canonical neural network model of [1].

Our work paves the way for exploring the role of sparse heterogeneous networks on the dynamics of ecosystems, coupled oscillators, epidemic spreading, and beyond. Future works include determining the phase diagram of the sparse Lotka-Volterra model [7], the influence of the external noise on phase diagrams [27], and the role of network heterogeneities on the critical exponents of complex systems [65, 69]. Equation (7) also forms the basis for calculating correlation functions [3] and deriving approximate dynamical equations for macroscopic order-parameters.

F. L. M. thanks Tuan Minh Pham for many stimulating discussions. The author also thanks Thomas Peron and Tuan Minh Pham for their valuable comments on the manuscript.

-
- [1] H. Sompolinsky, A. Crisanti, and H. J. Sommers, “Chaos in random neural networks,” *Phys. Rev. Lett.* **61**, 259–262 (1988).
- [2] Jonathan Kadmon and Haim Sompolinsky, “Transition to chaos in random neuronal networks,” *Phys. Rev. X* **5**, 041030 (2015).
- [3] Daniel Martí, Nicolas Brunel, and Srdjan Ostojic, “Correlations between synapses in pairs of neurons slow down dynamics in randomly connected neural networks,” *Phys. Rev. E* **97**, 062314 (2018).
- [4] A. Crisanti and H. Sompolinsky, “Path integral approach to random neural networks,” *Phys. Rev. E* **98**, 062120 (2018).
- [5] Carles Martorell, Rubén Calvo, Alessia Annibale, and Miguel A. Muñoz, “Dynamically selected steady states and criticality in non-reciprocal networks,” *Chaos, Solitons and Fractals* **182**, 114809 (2024).
- [6] Manfred Opper and Sigurd Diederich, “Phase transition and $1/f$ noise in a game dynamical model,” *Phys. Rev. Lett.* **69**, 1616–1619 (1992).
- [7] Guy Bunin, “Ecological communities with lotka-volterra dynamics,” *Phys. Rev. E* **95**, 042414 (2017).
- [8] Ada Altieri, Felix Roy, Chiara Cammarota, and Giulio Biroli, “Properties of equilibria and glassy phases of the random lotka-volterra model with demographic noise,” *Phys. Rev. Lett.* **126**, 258301 (2021).
- [9] Angélica S. Mata and Silvio C. Ferreira, “Pair quenched mean-field theory for the susceptible-infected-susceptible model on complex networks,” *Europhysics Letters* **103**, 48003 (2013).
- [10] P. Van Mieghem, “Epidemic phase transition of the sis type in networks,” *Europhysics Letters* **97**, 48004 (2012).
- [11] A. V. Goltsev, S. N. Dorogovtsev, J. G. Oliveira, and J. F. F. Mendes, “Localization and spreading of diseases in complex networks,” *Phys. Rev. Lett.* **109**, 128702 (2012).
- [12] Romualdo Pastor-Satorras, Claudio Castellano, Piet Van Mieghem, and Alessandro Vespignani, “Epidemic processes in complex networks,” *Rev. Mod. Phys.* **87**, 925–979 (2015).
- [13] J. C. Stiller and G. Radons, “Dynamics of nonlinear oscillators with random interactions,” *Phys. Rev. E* **58**, 1789–1799 (1998).
- [14] Francisco A. Rodrigues, Thomas K. DM. Peron, Peng Ji, and Jürgen Kurths, “The kuramoto model in complex networks,” *Physics Reports* **610**, 1–98 (2016), the Kuramoto model in complex networks.
- [15] Axel Prüser, Sebastian Rosmej, and Andreas Engel, “Nature of the volcano transition in the fully disordered kuramoto model,” *Phys. Rev. Lett.* **132**, 187201 (2024).
- [16] Fabian Baumann, Philipp Lorenz-Spreen, Igor M. Sokolov, and Michele Starnini, “Modeling echo chambers and polarization dynamics in social networks,” *Phys. Rev. Lett.* **124**, 048301 (2020).
- [17] Fabian Baumann, Philipp Lorenz-Spreen, Igor M. Sokolov, and Michele Starnini, “Emergence of polarized ideological opinions in multidimensional topic spaces,” *Phys. Rev. X* **11**, 011012 (2021).
- [18] Claude Godrèche and Jean-Marc Luck, “Characterising the nonequilibrium stationary states of ornstein-uhlenbeck processes,” *Journal of Physics A: Mathematical and Theoretical* **52**, 035002 (2018).
- [19] Andrea Crisanti and Matteo Paoluzzi, “Most probable path of active ornstein-uhlenbeck particles,” *Phys. Rev. E* **107**, 034110 (2023).
- [20] Francesco Ferraro, Christian Grilletta, Amos Maritan, Samir Suweis, and Sandro Azaele, “Exact solution of dynamical mean-field theory for a linear system with annealed disorder,” (2024), arXiv:2405.05183 [cond-mat.dis-nn].
- [21] V. Thibault, A. Allard, and P. Desrosiers, “The low-rank hypothesis of complex systems,” *Nat. Phys.* **20**, 294–302 (2024).
- [22] P. C. Martin, E. D. Siggia, and H. A. Rose, “Statistical dynamics of classical systems,” *Phys. Rev. A* **8**, 423–437 (1973).
- [23] A.C.C. Coolen, “Chapter 15 statistical mechanics of recurrent neural networks ii — dynamics,” in *Neuro-Informatics and Neural Modelling*, Handbook of Biological Physics, Vol. 4, edited by F. Moss and S. Gielen (North-Holland, 2001) pp. 619–684.
- [24] John A Hertz, Yasser Roudi, and Peter Sollich, “Path integral methods for the dynamics of stochastic and disordered systems,” *Journal of Physics A: Mathematical and Theoretical* **50**, 033001 (2016).
- [25] F Roy, G Biroli, G Bunin, and C Cammarota, “Numerical implementation of dynamical mean field theory for disordered systems: application to the lotka-volterra model of ecosystems,” *Journal of Physics A: Mathematical and Theoretical* **52**, 484001 (2019).
- [26] Tobias Galla, “Dynamically evolved community size and stability of random lotka-volterra ecosystems(a),” *Europhysics Letters* **123**, 48004 (2018).
- [27] Jannis Schuecker, Sven Goedeke, and Moritz Helias, “Optimal sequence memory in driven random networks,” *Phys. Rev. X* **8**, 041029 (2018).
- [28] Lyle Poley, Joseph W. Baron, and Tobias Galla, “Generalized lotka-volterra model with hierarchical interac-

- tions,” *Phys. Rev. E* **107**, 024313 (2023).
- [29] Fabián Aguirre-López, “Heterogeneous mean-field analysis of the generalized lotka-volterra model on a network,” (2024), arXiv:2404.11164 [cond-mat.dis-nn].
- [30] Jong Il Park, Deok-Sun Lee, Sang Hoon Lee, and Hye Jin Park, “Incorporating heterogeneous interactions for ecological biodiversity,” (2024), arXiv:2403.15730 [physics.bio-ph].
- [31] Tuan Minh Pham and Kunihiko Kaneko, “Dynamical theory for adaptive systems,” (2024), arXiv:2306.01403 [q-bio.PE].
- [32] Valentina Ros, Felix Roy, Giulio Biroli, and Guy Bunin, “Quenched complexity of equilibria for asymmetric generalized lotka–volterra equations,” *Journal of Physics A: Mathematical and Theoretical* **56**, 305003 (2023).
- [33] M. Newman, *Networks: An Introduction* (OUP Oxford, 2010).
- [34] Paulo R. Guimarães, “The structure of ecological networks across levels of organization,” *Annual Review of Ecology, Evolution, and Systematics* **51**, 433–460 (2020).
- [35] J P L Hatchett, B Wemmenhove, I Pérez Castillo, T Nikolettopoulos, N S Skantzos, and A C C Coolen, “Parallel dynamics of disordered ising spin systems on finitely connected random graphs,” *Journal of Physics A: Mathematical and General* **37**, 6201 (2004).
- [36] I Neri and D Bollé, “The cavity approach to parallel dynamics of ising spins on a graph,” *Journal of Statistical Mechanics: Theory and Experiment* **2009**, P08009 (2009).
- [37] Kazushi Mimura and A C C Coolen, “Parallel dynamics of disordered ising spin systems on finitely connected directed random graphs with arbitrary degree distributions,” *Journal of Physics A: Mathematical and Theoretical* **42**, 415001 (2009).
- [38] Yasser Roudi and John Hertz, “Dynamical tap equations for non-equilibrium ising spin glasses,” *Journal of Statistical Mechanics: Theory and Experiment* **2011**, P03031 (2011).
- [39] Erik Aurell and Hamed Mahmoudi, “Dynamic mean-field and cavity methods for diluted ising systems,” *Phys. Rev. E* **85**, 031119 (2012).
- [40] Gino Del Ferraro and Erik Aurell, “Dynamic message-passing approach for kinetic spin models with reversible dynamics,” *Phys. Rev. E* **92**, 010102 (2015).
- [41] E. Aurell, G. Del Ferraro, E. Domínguez, and R. Mulet, “Cavity master equation for the continuous time dynamics of discrete-spin models,” *Phys. Rev. E* **95**, 052119 (2017).
- [42] Eduardo Domínguez Vázquez, Gino Del Ferraro, and Federico Ricci-Tersenghi, “A simple analytical description of the non-stationary dynamics in ising spin systems,” *Journal of Statistical Mechanics: Theory and Experiment* **2017**, 033303 (2017).
- [43] Freya Behrens, Barbora Hudcová, and Lenka Zdeborová, “Backtracking dynamical cavity method,” *Phys. Rev. X* **13**, 031021 (2023).
- [44] Freya Behrens, Barbora Hudcová, and Lenka Zdeborová, “Dynamical phase transitions in graph cellular automata,” *Phys. Rev. E* **109**, 044312 (2024).
- [45] B. Derrida, E. Gardner, and A. Zippelius, “An exactly solvable asymmetric neural network model,” *Europhysics Letters* **4**, 167 (1987).
- [46] Malbor Asllani, Renaud Lambiotte, and Timoteo Carletti, “Structure and dynamical behavior of non-normal networks,” *Science Advances* **4**, eaau9403 (2018), <https://www.science.org/doi/pdf/10.1126/sciadv.aau9403>.
- [47] Yangfan Peng, Antje Bjelde, Pau Vilimelis Aceituno, Franz X. Mittermaier, Henrike Planert, Sabine Grosser, Julia Onken, Katharina Faust, Thilo Kalbhenn, Matthias Simon, Helena Radbruch, Pawel Fidzinski, Dietmar Schmitz, Henrik Alle, Martin Holtkamp, Imre Vida, Benjamin F. Grewe, and Jörg R. P. Geiger, “Directed and acyclic synaptic connectivity in the human layer 2-3 cortical microcircuit,” *Science* **384**, 338–343 (2024), <https://www.science.org/doi/pdf/10.1126/science.adg8828>.
- [48] Jennifer A. Dunne, Richard J. Williams, and Neo D. Martinez, “Food-web structure and network theory: The role of connectance and size,” *Proceedings of the National Academy of Sciences* **99**, 12917–12922 (2002), <https://www.pnas.org/doi/pdf/10.1073/pnas.192407699>.
- [49] Jordi Bascompte, “Disentangling the web of life,” *Science* **325**, 416–419 (2009), <https://www.science.org/doi/pdf/10.1126/science.1170749>.
- [50] M Mézard and G Parisi, “The bethe lattice spin glass revisited,” *Eur. Phys. J. B* **20**, 217–233 (2001).
- [51] M Mézard and G Parisi, “The cavity method at zero temperature,” *J. Stat. Phys.* **111**, 1–34 (2003).
- [52] Reimer Kühn, “Spectra of sparse random matrices,” *Journal of Physics A: Mathematical and Theoretical* **41**, 295002 (2008).
- [53] Fernando Lucas Metz, Izaak Neri, and Tim Rogers, “Spectral theory of sparse non-hermitian random matrices,” *Journal of Physics A: Mathematical and Theoretical* **52**, 434003 (2019).
- [54] R Abou-Chacra, D J Thouless, and P W Anderson, “A selfconsistent theory of localization,” *Journal of Physics C: Solid State Physics* **6**, 1734 (1973).
- [55] M. Mézard and A. Montanari, *Information, Physics, and Computation*, Oxford Graduate Texts (OUP Oxford, 2009).
- [56] Izaak Neri and Fernando Lucas Metz, “Eigenvalue outliers of non-hermitian random matrices with a local tree structure,” *Phys. Rev. Lett.* **117**, 224101 (2016).
- [57] Izaak Neri and Fernando Lucas Metz, “Linear stability analysis of large dynamical systems on random directed graphs,” *Phys. Rev. Res.* **2**, 033313 (2020).
- [58] Fernando Lucas Metz and Izaak Neri, “Localization and universality of eigenvectors in directed random graphs,” *Phys. Rev. Lett.* **126**, 040604 (2021).
- [59] M. E. J. Newman, S. H. Strogatz, and D. J. Watts, “Random graphs with arbitrary degree distributions and their applications,” *Phys. Rev. E* **64**, 026118 (2001).
- [60] Bailey K. Fosdick, Daniel B. Larremore, Joel Nishimura, and Johan Ugander, “Configuring random graph models with fixed degree sequences,” *SIAM Review* **60**, 315–355 (2018), <https://doi.org/10.1137/16M1087175>.
- [61] Fernando Lucas Metz, “Supplemental material,” .
- [62] Fernando L. Metz and Jeferson D. Silva, “Spectral density of dense random networks and the breakdown of the wigner semicircle law,” *Phys. Rev. Res.* **2**, 043116 (2020).
- [63] Fernando L Metz and Thomas Peron, “Mean-field theory of vector spin models on networks with arbitrary degree distributions,” *Journal of Physics: Complexity* **3**, 015008 (2022).
- [64] Jeferson D Silva and Fernando L Metz, “Analytic solution of the resolvent equations for heterogeneous random graphs: spectral and localization properties,” *Journal of Physics: Complexity* **3**, 045012 (2022).

- [65] Leonardo S. Ferreira and Fernando L. Metz, “Nonequilibrium dynamics of the ising model on heterogeneous networks with an arbitrary distribution of threshold noise,” *Phys. Rev. E* **107**, 034127 (2023).
- [66] G. Timár, A. V. Goltsev, S. N. Dorogovtsev, and J. F. F. Mendes, “Mapping the structure of directed networks: Beyond the bow-tie diagram,” *Phys. Rev. Lett.* **118**, 078301 (2017).
- [67] G.L. Baker and J.P. Gollub, *Chaotic Dynamics: An Introduction* (Cambridge University Press, 1996).
- [68] H. Nishimori, *Statistical Physics of Spin Glasses and Information Processing: An Introduction*, International series of monographs on physics (Oxford University Press, 2001).
- [69] Thibaut Arnoult de Pirey and Guy Bunin, “Critical behavior of a phase transition in the dynamics of interacting populations,” (2024), arXiv:2402.05063 [cond-mat.stat-mech].

Supplemental material for “Dynamical mean-field theory of complex systems on
sparse directed networks”

Fernando L. Metz

Physics Institute, Federal University of Rio Grande do Sul, 91501-970 Porto Alegre, Brazil

(Dated: June 11, 2024)

arXiv:2406.06346v1 [cond-mat.dis-nn] 10 Jun 2024

I. INTRODUCTION

In this supplemental material, we show how to apply dynamical mean-field theory (DMFT) to solve nonlinear systems of coupled differential equations governing a broad range of dynamical processes on sparse directed graphs. The microscopic variables $x_1(t), \dots, x_N(t)$ evolve in time according to the coupled differential equations

$$\dot{x}_i(t) = -f(x_i) + \sum_{j=1}^N C_{ij} J_{ij} g(x_i, x_j) + h_i(t) + \xi_i(t), \quad (1)$$

with $i = 1, \dots, N$. The variable $\xi_i(t)$ represents an uncorrelated Gaussian noise with mean zero and variance σ^2 . Unlike the model definitions in the main text, here we have included, for technical purposes, an external field $h_i(t)$ in the dynamical equations, which will be set to zero at the end of the calculation. The functions $f(x)$ and $g(x, x')$ specify the model under study. Table I of the main text shows five paradigmatic examples of complex systems modeled by Eq. (1).

The binary variable $C_{ij} \in \{0, 1\}$ tells us whether there is a directed edge pointing from node j to node i in the network, while J_{ij} represents the strength of the directed interaction $j \rightarrow i$. We set $C_{ii} = 0$. The off-diagonal entries $\{C_{ij}\}_{i \neq j}$ encode the network topology, and they are drawn from the joint probability distribution

$$\mathbb{P}(\{C_{ij}\}) = \frac{1}{\mathcal{N}} \prod_{i \neq j=1}^N \left[\frac{c}{N} \delta_{C_{ij}, 1} + \left(1 - \frac{c}{N}\right) \delta_{C_{ij}, 0} \right] \prod_{i=1}^N \delta_{K_i, \sum_{j=1}^N C_{ij}} \delta_{L_i, \sum_{j=1}^N C_{ji}}, \quad (2)$$

where \mathcal{N} is the normalization factor. The local variables $K_i = \sum_{j=1}^N C_{ij}$ and $L_i = \sum_{j=1}^N C_{ji}$ denote, respectively, the indegree and the outdegree of node i . The joint probability distribution of indegrees k and outdegrees ℓ is formally defined as

$$p_{k,\ell} = \lim_{N \rightarrow \infty} \frac{1}{N} \sum_{i=1}^N \delta_{K_i, k} \delta_{L_i, \ell}, \quad (3)$$

while the mean degree c is given by

$$c = \sum_{k,\ell=0}^{\infty} k p_{k,\ell} = \sum_{k,\ell=0}^{\infty} \ell p_{k,\ell}. \quad (4)$$

The parameter c controls the average number of links that enter or leave a node. The distribution of Eq. (2) defines an ensemble of directed random networks in which a directed link $j \rightarrow i$ is randomly placed between nodes i and j with probability c/N , subject to the local constraints imposed by the prescribed degree sequences K_1, \dots, K_N and L_1, \dots, L_N .

The degrees at different nodes are independent and identically distributed random variables drawn from the joint distribution $p_{k,\ell}$. However, the pair of degrees (K_i, L_i) at node i might be correlated. If K_i and L_i are statistically independent, then the joint degree distribution $p_{k,\ell}$ factorizes as $p_{k,\ell} = p_{\text{in},k} p_{\text{out},\ell}$. Here we solve the dynamics for an arbitrary $p_{k,\ell}$, while in the main text we present the final solution for the factorized case $p_{k,\ell} = p_{\text{in},k} p_{\text{out},\ell}$. The coupling strengths $\{J_{ij}\}$ are independent and identically distributed random variables drawn from an arbitrary distribution p_J with mean μ_J and variance σ_J^2 . Thus, the distributions $p_{k,\ell}$ and p_J fully specify the ensemble of networks.

In the next section, we detail how to solve the current model, in the limit $N \rightarrow \infty$, using dynamical mean-field theory (DMFT). We emphasize that we solve the model for *finite* c , which characterizes a genuine sparse interacting system, where the average number of edges per node remains finite in the thermodynamic limit. As we show below, the main outcome of DMFT for finite c is a self-consistent equation for the path-probability $\mathcal{P}[x]$ encoding the effective dynamics of a single dynamical variable. The solution of this equation not only allows to compute macroscopic observables, but it also enables to follow the time-evolution of the full probability distribution of the microscopic degrees of freedom. In section III, we explain how to generalize the population dynamics approach [1–3] to solve the self-consistent equation for the path-probability $\mathcal{P}[x]$. We also present a detailed account of the algorithm, which we hope will be useful for future works. Finally, in section IV, we calculate the high-connectivity limit $c \rightarrow \infty$ of $\mathcal{P}[x]$ and discuss its convergence towards fully-connected models. In particular, we show that fully-connected models are recovered if the variance of rescaled degrees goes to zero. In other words, fully-connected models are not universal with respect to degree fluctuations.

II. DYNAMICAL MEAN-FIELD THEORY FOR MODELS ON SPARSE DIRECTED NETWORKS

In this section we explain how to solve the dynamics of the model in the limit $N \rightarrow \infty$ using dynamical mean-field theory. Let $\mathbf{x}(t) = (x_1(t), \dots, x_N(t))$ denote the global state of the system at time t , and let $\mathcal{P}[\mathbf{x}]$ be the functional probability density of observing a continuous trajectory of the global state $\mathbf{x}(t)$ in a finite time interval. The path-probability $\mathcal{P}[\mathbf{x}]$ can be formally written as

$$\mathcal{P}[\mathbf{x}] = \int \left(\prod_{i=1}^N D\xi_i \right) \mathcal{P}_\sigma[\boldsymbol{\xi}] \prod_{i=1}^N \delta_F \left[\dot{x}_i + f(x_i) - \sum_{j=1}^N C_{ij} J_{ij} g(x_i, x_j) - h_i(t) + \xi_i(t) \right], \quad (5)$$

where δ_F is a Dirac- δ functional, and the symbol Dx represents a functional integration measure over all possible functions $x(t)$ in the prescribed time domain. The object $\mathcal{P}_\sigma[\boldsymbol{\xi}]$ is the path-probability of the Gaussian noise

$$\mathcal{P}_\sigma[\boldsymbol{\xi}] = \frac{1}{\mathcal{N}_\sigma} \exp \left(-\frac{1}{2\sigma^2} \int dt \sum_{i=1}^N (\xi_i(t))^2 \right), \quad (6)$$

with \mathcal{N}_σ the normalization constant. The integrals over time run over a fixed time interval, but we omit the limits of integration, here and elsewhere, for the sake of simplifying the notation. The starting point of DMFT is the introduction of the generating functional $\mathcal{Z}[\boldsymbol{\psi}, \mathbf{h}]$ of the path-probability $\mathcal{P}[\mathbf{x}]$,

$$\mathcal{Z}[\boldsymbol{\psi}, \mathbf{h}] = \int \left(\prod_{i=1}^N Dx_i \right) \mathcal{P}[\mathbf{x}] e^{i \int dt \sum_{i=1}^N x_i(t) \psi_i(t)}, \quad (7)$$

where $\boldsymbol{\psi}(t) = (\psi_1(t), \dots, \psi_N(t))$ and $\mathbf{h}(t) = (h_1(t), \dots, h_N(t))$. The derivatives of $\mathcal{Z}[\boldsymbol{\psi}, \mathbf{h}]$ with respect to the auxiliary sources $\psi_1(t), \dots, \psi_N(t)$ yield the average of products of $x_1(t), \dots, x_N(t)$ over the dynamical process specified by Eq. (1). For instance, the moments of $x_i(t)$ in the absence of external fields ($h_i(t) = 0$) follow from

$$\langle x_i^n(t) \rangle = (-i)^n \lim_{\boldsymbol{\psi} \rightarrow 0} \lim_{\mathbf{h} \rightarrow 0} \frac{\delta^n \mathcal{Z}[\boldsymbol{\psi}, \mathbf{h}]}{\delta \psi_i^n(t)}. \quad (8)$$

In particular, the first two moments yield the time-evolution of the following macroscopic observables

$$m(t) = \lim_{N \rightarrow \infty} \frac{1}{N} \sum_{i=1}^N \langle x_i(t) \rangle, \quad (9)$$

$$q(t) = \lim_{N \rightarrow \infty} \frac{1}{N} \sum_{i=1}^N \langle x_i^2(t) \rangle. \quad (10)$$

By construction, the generating functional fulfills the normalization condition $\mathcal{Z}[0, \mathbf{h}] = 1$.

By inserting Eq. (5) into the definition of $\mathcal{Z}[\boldsymbol{\psi}, \mathbf{h}]$, using a functional integral representation of δ_F , and then integrating over the Gaussian noise $\boldsymbol{\xi}(t)$, one derives the following expression

$$\mathcal{Z}[\boldsymbol{\psi}, \mathbf{h}] = \int \left(\prod_{i=1}^N Dx_i D\hat{x}_i \right) \exp \left(-i \sum_{i \neq j=1}^N C_{ij} J_{ij} \int dt \hat{x}_i(t) g(x_i(t), x_j(t)) + i \int dt \sum_{i=1}^N S_i(x_i(t), \hat{x}_i(t), h_i(t), \psi_i(t)) \right), \quad (11)$$

where the single-site action S_i is defined as

$$S_i[x_i(t), \hat{x}_i(t), h_i(t), \psi_i(t)] = x_i(t) \psi_i(t) + \frac{i\sigma}{2} \hat{x}_i^2(t) + \hat{x}_i(t) [\dot{x}_i(t) + f(x_i(t)) - h_i(t)]. \quad (12)$$

According to Eq. (11), the external sources $h_i(t)$ and $\psi_i(t)$ are coupled, respectively, to the dynamical variables $\hat{x}_i(t)$ and $x_i(t)$ at node i . As we show below, both fields $h_i(t)$ and $\psi_i(t)$ are important to simplify the saddle-point equations and identify the physical meaning of the order-parameters.

A. The saddle-point integral

The aim of DMFT is to compute, in the limit $N \rightarrow \infty$, the disorder averaged generating functional, $\langle \mathcal{Z}[\boldsymbol{\psi}, \mathbf{h}] \rangle_{\{C_{ij}, J_{ij}\}}$. The symbol $\langle \dots \rangle_{\{C_{ij}, J_{ij}\}}$ represents the average over both the graph structure $\{C_{ij}\}$ and the coupling strengths $\{J_{ij}\}$. In this subsection, we explain how to reduce the calculation of $\langle \mathcal{Z}[\boldsymbol{\psi}, \mathbf{h}] \rangle_{\{C_{ij}, J_{ij}\}}$ to the solution of a saddle-point integral in the limit $N \rightarrow \infty$.

By taking the average of Eq. (11) over $\{C_{ij}\}$ and $\{J_{ij}\}$, we can write $\langle \mathcal{Z}[\boldsymbol{\psi}, \mathbf{h}] \rangle_{\{C_{ij}, J_{ij}\}}$ as follows

$$\langle \mathcal{Z}[\boldsymbol{\psi}, \mathbf{h}] \rangle_{\{C_{ij}, J_{ij}\}} = \int \left(\prod_{i=1}^N Dx_i D\hat{x}_i \right) \mathcal{F}[\mathbf{x}, \hat{\mathbf{x}}] \exp \left(i \int dt \sum_{i=1}^N S_i(x_i(t), \hat{x}_i(t), h_i(t), \psi_i(t)) \right), \quad (13)$$

where

$$\mathcal{F}[\mathbf{x}, \hat{\mathbf{x}}] = \left\langle \prod_{i \neq j=1}^N \exp \left(-i C_{ij} J_{ij} \int dt \hat{x}_i(t) g(x_i(t), x_j(t)) \right) \right\rangle_{\{C_{ij}, J_{ij}\}}. \quad (14)$$

By using the integral representation of the Kronecker- δ

$$\delta_{n,m} = \int_0^{2\pi} \frac{du}{2\pi} \exp[iu(n-m)] \quad (n, m \in \mathbb{N}), \quad (15)$$

we can factorize the joint distribution $\mathbb{P}(\{C_{ij}\})$, Eq. (2), in terms of a product over pairs of nodes

$$\mathbb{P}(\{C_{ij}\}) = \frac{1}{N} \int_0^{2\pi} \left(\frac{du_i dv_i}{4\pi^2} \right) e^{i \sum_{i=1}^N (K_i u_i + L_i v_i)} \prod_{i \neq j=1}^N \left[\frac{c}{N} \delta_{C_{ij}, 1} + \left(1 - \frac{c}{N} \right) \delta_{C_{ij}, 0} \right] e^{-C_{ij}(u_i + v_j)}. \quad (16)$$

This expression for $\mathbb{P}(\{C_{ij}\})$ allows us to calculate the average over $\{C_{ij}\}$ in Eq. (14), leading to the result

$$\mathcal{F}[\mathbf{x}, \hat{\mathbf{x}}] \simeq \int_0^{2\pi} \left(\prod_{i=1}^N \frac{du_i dv_i}{4\pi^2} \right) \exp \left(i \sum_{i=1}^N (u_i K_i + v_i L_i) + \frac{c}{N} \sum_{ij=1}^N e^{-i(u_i + v_j)} \left\langle e^{-iJ \int dt \hat{x}_i(t) g(x_i(t), x_j(t))} \right\rangle_J \right), \quad (17)$$

valid for large N . We have retained only terms of $\mathcal{O}(N)$ in the exponent of Eq. (17), since these are precisely the terms that will contribute to the solution of the saddle-point integral for $N \rightarrow \infty$. In addition, irrelevant terms that are independent of $\{\hat{x}_i(t), x_i(t)\}$ have been neglected when writing Eq. (17). The symbol $\langle \dots \rangle_J$ denotes the average over the coupling strength J between a single pair of nodes.

In contrast to fully-connected Gaussian models, where the disorder average of $\mathcal{Z}[\boldsymbol{\psi}, \mathbf{h}]$ yields a quadratic functional of the dynamical variables [4, 5], here the exponent in Eq. (17) contains an exponential functional of $\{\hat{x}_i(t), x_i(t)\}$. This non-quadratic behaviour renders the problem technically more challenging in comparison to fully-connected models. In spite of that, we can still decouple sites by introducing the functional order-parameters

$$P[x] = \frac{1}{N} \sum_{i=1}^N \delta_F[x(t) - x_i(t)] e^{-iv_i},$$

$$W[x, \hat{x}] = \frac{1}{N} \sum_{i=1}^N \delta_F[x(t) - x_i(t)] \delta_F[\hat{x}(t) - \hat{x}_i(t)] e^{-iu_i}.$$

Indeed, substituting Eq. (17) in Eq. (13), we can write $\langle \mathcal{Z}[\boldsymbol{\psi}, \mathbf{h}] \rangle_{\{C_{ij}, J_{ij}\}}$ as a functional integral over $P[x]$ and $W[x, \hat{x}]$, namely

$$\begin{aligned} \langle \mathcal{Z}[\boldsymbol{\psi}, \mathbf{h}] \rangle_{\{C_{ij}, J_{ij}\}} &\simeq \int \left(\prod_{i=1}^N Dx_i D\hat{x}_i \right) \int_0^{2\pi} \left(\prod_{i=1}^N \frac{du_i dv_i}{4\pi^2} \right) e^{i \int dt \sum_{i=1}^N S_i(x_i(t), \hat{x}_i(t), h_i(t), \psi_i(t)) + i \sum_{i=1}^N (u_i K_i + v_i L_i)} \\ &\times \int DP DW \delta_F \left[P[x] - \frac{1}{N} \sum_{i=1}^N \delta_F[x(t) - x_i(t)] e^{-iv_i} \right] \delta_F \left[W[x, \hat{x}] - \frac{1}{N} \sum_{i=1}^N \delta_F[x(t) - x_i(t)] \delta_F[\hat{x}(t) - \hat{x}_i(t)] e^{-iu_i} \right] \\ &\times \exp \left(cN \int Dx D\hat{x}' D\hat{x} W[x, \hat{x}] P[x'] \left\langle e^{-iJ \int dt \hat{x}(t) g(x(t), x'(t))} \right\rangle_J \right). \end{aligned} \quad (18)$$

By introducing the conjugate order-parameters $\hat{P}[x]$ and $\hat{W}[x, \hat{x}]$ by means of the functional Fourier transforms,

$$\delta_F \left[P[x] - \frac{1}{N} \sum_{i=1}^N \delta_F [x(t) - x_i(t)] e^{-iv_i} \right] = \int D\hat{P} e^{i \int D x \hat{P}[x] P[x] - \frac{i}{N} \sum_{i=1}^N \hat{P}[x_i] e^{-iv_i}},$$

$$\delta_F \left[W[x, \hat{x}] - \frac{1}{N} \sum_{i=1}^N \delta_F [x(t) - x_i(t)] \delta_F [\hat{x}(t) - \hat{x}_i(t)] e^{-iu_i} \right] = \int D\hat{W} e^{i \int D x D \hat{x} \hat{W}[x, \hat{x}] W[x, \hat{x}] - \frac{i}{N} \sum_{i=1}^N \hat{W}[x_i, \hat{x}_i] e^{-iu_i}},$$

we are able to factorize the exponent of Eq. (18) as a sum of single-site functionals, yielding

$$\langle \mathcal{Z}[\boldsymbol{\psi}, \mathbf{h}] \rangle_{\{C_{ij}, J_{ij}\}} \simeq \int D P D \hat{P} D W D \hat{W} \exp \left(i \int D x \hat{P}[x] P[x] + i \int D x D \hat{x} \hat{W}[x, \hat{x}] W[x, \hat{x}] \right) \quad (19)$$

$$\times \exp \left(c N \int D x D x' D \hat{x} W[x, \hat{x}] P[x'] \left\langle e^{-iJ \int dt \hat{x}(t) g(x(t), x'(t))} \right\rangle_J \right)$$

$$\times \exp \left[\sum_{i=1}^N \ln \left(\int D x D \hat{x} \int \frac{d u d v}{4\pi^2} e^{i \int dt S_i(x(t), \hat{x}(t), \psi_i(t), h_i(t)) + i(u K_i + v L_i) - \frac{i}{N} e^{-iv} \hat{P}[x] - \frac{i}{N} e^{-iu} \hat{W}[x, \hat{x}]} \right) \right]. \quad (20)$$

Finally, we use the power-series representations

$$\exp \left(-\frac{i}{N} e^{-iv} \hat{P}[x] \right) = \sum_{r=0}^{\infty} \frac{1}{r!} \left(-\frac{i}{N} \right)^r \left(\hat{P}[x] \right)^r e^{-ivr} \quad (21)$$

and

$$\exp \left(-\frac{i}{N} e^{-iu} \hat{W}[x, \hat{x}] \right) = \sum_{r=0}^{\infty} \frac{1}{r!} \left(-\frac{i}{N} \right)^r \left(\hat{W}[x, \hat{x}] \right)^r e^{-iur}, \quad (22)$$

which enables to integrate over u and v in Eq. (20). By rescaling the conjugate order-parameters in the resulting expression as $\hat{P}[x] \rightarrow N\hat{P}[x]$ and $\hat{W}[x, \hat{x}] \rightarrow N\hat{W}[x, \hat{x}]$, we can express $\langle \mathcal{Z}[\boldsymbol{\psi}, \mathbf{h}] \rangle_{\{C_{ij}, J_{ij}\}}$ as an integral over the order-parameters

$$\langle \mathcal{Z}[\boldsymbol{\psi}, \mathbf{h}] \rangle_{\{C_{ij}, J_{ij}\}} \simeq \int D P D \hat{P} D W D \hat{W} e^{N\Phi[P, \hat{P}, W, \hat{W}]}, \quad (23)$$

with

$$\Phi[P, \hat{P}, W, \hat{W}] = i \int D x \hat{P}[x] P[x] + i \int D x D \hat{x} \hat{W}[x, \hat{x}] W[x, \hat{x}] + c \int D x D x' D \hat{x} W[x, \hat{x}] P[x'] \left\langle e^{-iJ \int dt \hat{x}(t) g(x(t), x'(t))} \right\rangle_J$$

$$+ \frac{1}{N} \sum_{i=1}^N \ln \left[\int D x D \hat{x} e^{i \int dt S_i(x(t), \hat{x}(t), \psi_i(t), h_i(t))} \left(-i\hat{P}[x] \right)^{L_i} \left(-i\hat{W}[x, \hat{x}] \right)^{K_i} \right]. \quad (24)$$

Now we can find the asymptotic behaviour of the integral in Eq. (23) using the saddle-point method. In the limit $N \rightarrow \infty$, the integral is dominated by the stationary points of $\Phi[P, \hat{P}, W, \hat{W}]$,

$$\langle \mathcal{Z}[\boldsymbol{\psi}, \mathbf{h}] \rangle_{\{C_{ij}, J_{ij}\}} \simeq e^{N\Phi[P_s, \hat{P}_s, W_s, \hat{W}_s]}, \quad (25)$$

where the functional order-parameters that extremize $\Phi[P, \hat{P}, W, \hat{W}]$ fulfill the saddle-point equations

$$P_s[x] = \frac{1}{N} \sum_{i=1}^N \frac{L_i}{B_i[h_i, \psi_i]} \left(-i\hat{P}_s[x] \right)^{L_i-1} \int D \hat{x} \left(-i\hat{W}_s[x, \hat{x}] \right)^{K_i} e^{i \int dt S_i(x(t), \hat{x}(t), \psi_i(t), h_i(t))}, \quad (26)$$

$$W_s[x, \hat{x}] = \frac{1}{N} \sum_{i=1}^N \frac{K_i}{B_i[h_i, \psi_i]} \left(-i\hat{W}_s[x, \hat{x}] \right)^{K_i-1} \left(-i\hat{P}_s[x] \right)^{L_i} e^{i \int dt S_i(x(t), \hat{x}(t), \psi_i(t), h_i(t))}, \quad (27)$$

$$\hat{P}_s[x] = ic \int D x' D \hat{x} W_s[x', \hat{x}] \left\langle e^{-iJ \int dt \hat{x}(t) g(x'(t), x(t))} \right\rangle_J, \quad (28)$$

$$\hat{W}_s[x, \hat{x}] = ic \int D x' P_s[x'] \left\langle e^{-iJ \int dt \hat{x}(t) g(x(t), x'(t))} \right\rangle_J, \quad (29)$$

with

$$B_i[h_i, \psi_i] = \int Dx D\hat{x} e^{i \int dt S_i(x(t), \hat{x}(t), \psi_i(t), h_i(t))} \left(-i\hat{P}_s[x]\right)^{L_i} \left(-i\hat{W}_s[x, \hat{x}]\right)^{K_i}. \quad (30)$$

The self-consistent Eqs. (26-29) are derived from the application of the stationarity conditions

$$\frac{\delta\Phi}{\delta P[x]} \Big|_s = \frac{\delta\Phi}{\delta \hat{P}[x]} \Big|_s = \frac{\delta\Phi}{\delta W[x, \hat{x}]} \Big|_s = \frac{\delta\Phi}{\delta \hat{W}[x, \hat{x}]} \Big|_s = 0, \quad (31)$$

where the notation $(\dots)|_s$ means that $P[x] = P_s[x]$, $\hat{P}[x] = \hat{P}_s[x]$, $W[x, \hat{x}] = W_s[x, \hat{x}]$ and $\hat{W}[x, \hat{x}] = \hat{W}_s[x, \hat{x}]$.

B. Physical interpretation of the order-parameters

Now we explain how to distill the physical interpretation of the functional order-parameters, which plays a crucial role in simplifying the saddle-point equations. In addition, we show how Eqs. (26-29) can be reduced to a pair of self-consistent equations for the path-probability that determines the effective dynamics of a single degree of freedom.

First, we set $\psi_i(t) = h_i(t) = 0$ in the single-site action $S_i[x(t), \hat{x}(t), \psi_i(t), h_i(t)]$ and define the following normalized functional

$$\gamma[x, \hat{x}|k, \ell] = \frac{e^{i \int dt S(x(t), \hat{x}(t))} \left(-i\hat{P}_s[x]\right)^\ell \left(-i\hat{W}_s[x, \hat{x}]\right)^k}{\int Dx D\hat{x} e^{i \int dt S(x(t), \hat{x}(t))} \left(-i\hat{P}_s[x]\right)^\ell \left(-i\hat{W}_s[x, \hat{x}]\right)^k} \quad (32)$$

for fixed indegree k and outdegree ℓ . Our first task is to find out what is the physical interpretation of the above object. With that in mind, we take the derivative of Eq. (25) with respect to $\psi_i(t)$ and then we set $\psi_i(t) = h_i(t) = 0$, namely

$$\lim_{h \rightarrow 0} \lim_{\psi \rightarrow 0} \frac{\delta \langle \mathcal{Z}[\boldsymbol{\psi}, \mathbf{h}] \rangle_{\{C_{ij}, J_{ij}\}}}{\delta \psi_i(t)} = i \int Dx D\hat{x} x(t) \gamma[x, \hat{x}|K_i, L_i]. \quad (33)$$

Comparing the above expression with the first moment $\langle x_i(t) \rangle$ defined in Eq. (8), we conclude that

$$\mathcal{P}[x|k, \ell] = \int D\hat{x} \gamma[x, \hat{x}|k, \ell] \quad (34)$$

is the path-probability describing the effective dynamics of a single variable $x(t)$ conditioned to the indegree k and outdegree ℓ . Clearly, the path-probability $\mathcal{P}[x]$ of observing a dynamical trajectory of $x(t)$ is obtained by averaging $\mathcal{P}[x|k, \ell]$ over the joint degree distribution

$$\mathcal{P}[x] = \sum_{k, \ell=0} p_{k, \ell} \mathcal{P}[x|k, \ell]. \quad (35)$$

Equation (35) defines the central object of dynamical mean-field theory, as $\mathcal{P}[x]$ determines the effective dynamics of a single degree of freedom in the thermodynamic limit $N \rightarrow \infty$.

Let us derive a self-consistent equation for $\mathcal{P}[x]$. The first step consists in relating the functional probability densities, $\mathcal{P}[x|k, \ell]$ and $\gamma[x, \hat{x}|k, \ell]$, to the functional order-parameters using the saddle-point equations of the previous section. By setting $\psi_i(t) = h_i(t) = 0$ in Eqs. (26) and (28), we obtain the following relation

$$-iP_s[x] \hat{P}_s[x] = \sum_{k, \ell=0}^{\infty} \ell p_{k, \ell} \mathcal{P}[x|k, \ell]. \quad (36)$$

Similarly, combining Eqs. (27) and (29) for $\psi_i(t) = h_i(t) = 0$, we find

$$-iW_s[x, \hat{x}] \hat{W}_s[x, \hat{x}] = \sum_{k, \ell=0}^{\infty} k p_{k, \ell} \gamma[x, \hat{x}|k, \ell]. \quad (37)$$

Let us now infer the functional form of $\gamma[x, \hat{x}|k, \ell]$. This quantity gives the joint probability density of $x(t)$ and $\hat{x}(t)$ conditioned to the indegree k and outdegree ℓ . By taking the derivative of Eq. (25) with respect to $h_i(t)$ and then setting $\psi_i(t) = h_i(t) = 0$, we find the identity

$$\lim_{h \rightarrow 0} \lim_{\psi \rightarrow 0} \frac{\delta \langle \mathcal{Z}[\boldsymbol{\psi}, \mathbf{h}] \rangle_{\{C_{ij}, J_{ij}\}}}{\delta h_i(t)} = -i \int Dx D\hat{x} \hat{x}(t) \gamma[x, \hat{x}|K_i, L_i]. \quad (38)$$

Since $\mathcal{Z}[0, \mathbf{h}] = 1$, we conclude that

$$\int Dx D\hat{x} \hat{x}(t) \gamma[x, \hat{x}|K_i, L_i] = 0, \quad (39)$$

for arbitrary degrees K_i and L_i . By computing the second derivative of Eq. (25) with respect to $h_i(t)$ and using a similar argument, it is straightforward to show that the covariance of $\hat{x}(t)$ and $\hat{x}(t')$ fulfills

$$\int Dx D\hat{x} \hat{x}(t) \hat{x}(t') \gamma[x, \hat{x}|K_i, L_i] = 0. \quad (40)$$

Equations (39) and (40) are already enough to conclude that the marginal of $\gamma[x, \hat{x}|k, \ell]$ with respect to $x(t)$ fulfills the relation

$$\int Dx \gamma[x, \hat{x}|k, \ell] = \delta_F[\hat{x}]. \quad (41)$$

Thus, by combining Eqs. (34) and (41), we infer that $\gamma[x, \hat{x}|k, \ell]$ must be given by

$$\gamma[x, \hat{x}|k, \ell] = \mathcal{P}[x|k, \ell] \delta_F[\hat{x}]. \quad (42)$$

The derivation of the above factorized form of $\gamma[x, \hat{x}|k, \ell]$ is probably the most important step of this calculation, since it enables to simplify the saddle-point equations.

Now we are ready to derive the self-consistent equation for the path-probability for the effective dynamics of a single variable. Plugging Eq. (42) in (37) and using Eq. (29), we get

$$W_s[x, \hat{x}] = \frac{\delta_F[\hat{x}] \sum_{k, \ell=0}^{\infty} k p_{k, \ell} \mathcal{P}[x|k, \ell]}{c \int Dx' P_s[x'] \langle e^{-iJ \int dt \hat{x}(t) g(x(t), x'(t))} \rangle_J}. \quad (43)$$

The above expression allows us to considerably simplify Eq. (28) and obtain

$$\hat{P}_s[x] = \frac{ic}{\mathcal{N}_P}, \quad (44)$$

with the constant

$$\mathcal{N}_P = \int Dx P_s[x]. \quad (45)$$

Inserting Eqs. (29) and (44) into the right hand side of Eq. (34), and performing the functional integral over $\hat{x}(t)$, we can write the conditioned path-probability as follows

$$\begin{aligned} \mathcal{P}[x|k, \ell] &= \frac{c^{\ell+k}}{\mathcal{N}_{k, \ell} \mathcal{N}_P^\ell} \int \left(\prod_{j=1}^k Dx_j P_s[x_j] \right) \int \left(\prod_{j=1}^k dJ_j p_J(J_j) \right) \\ &\times \int D\xi \mathcal{P}_\sigma[\xi] \delta_F \left[\dot{x}(t) + f(x(t)) - \sum_{j=1}^k J_j g(x(t), x_j(t)) - \xi(t) \right], \end{aligned} \quad (46)$$

where $\mathcal{N}_{k, \ell}$ is the denominator of $\gamma[x, \hat{x}|k, \ell]$ (see Eq. (32)),

$$\mathcal{N}_{k, \ell} = \int Dx D\hat{x} e^{i \int dt S[x(t), \hat{x}(t)]} \left(-i \hat{P}_s[x] \right)^\ell \left(-i \hat{W}_s[x, \hat{x}] \right)^k, \quad (47)$$

and $\mathcal{P}_\sigma[\xi]$ is the functional probability distribution of the uncorrelated Gaussian noise $\xi(t)$ with mean zero and variance σ^2 . If we integrate over $x(t)$ on both sides of Eq. (46), we find a relation between $\mathcal{N}_{k,\ell}$ and \mathcal{N}_P ,

$$\mathcal{N}_{k,\ell} = c^{\ell+k} \mathcal{N}_P^{k-\ell}, \quad (48)$$

which enables to rewrite Eq. (46) as follows

$$\mathcal{P}[x|k,\ell] = \int \left(\prod_{j=1}^k Dx_j \mathcal{Q}[x_j] \right) \int \left(\prod_{j=1}^k dJ_j p_J(J_j) \right) \int D\xi \mathcal{P}_\sigma[\xi] \delta_F \left[\dot{x}(t) + f(x(t)) - \sum_{j=1}^k J_j g(x(t), x_j(t)) - \xi(t) \right], \quad (49)$$

with $\mathcal{Q}[x] = P_s[x]/\mathcal{N}_P$ representing a normalized functional of $x(t)$. The final step consists in identifying the physical meaning of $\mathcal{Q}[x]$, which is easily achieved by substituting Eq. (44) in the left hand side of Eq. (36),

$$\mathcal{Q}[x] = \sum_{k,\ell=0}^{\infty} \frac{lp_{k,\ell}}{c} \mathcal{P}[x|k,\ell]. \quad (50)$$

Therefore, $\mathcal{Q}[x]$ is the average of the conditioned path-probability $\mathcal{P}[x|k,\ell]$ over the degrees k and ℓ , which are sampled from the joint distribution $\frac{lp_{k,\ell}}{c}$. Plugging Eq. (49) in the above expression leads to the self-consistent equation for $\mathcal{Q}[x]$

$$\mathcal{Q}[x] = \sum_{k,\ell=0}^{\infty} \frac{lp_{k,\ell}}{c} \int \left(\prod_{j=1}^k Dx_j \mathcal{Q}[x_j] \right) \int \left(\prod_{j=1}^k dJ_j p_J(J_j) \right) \int D\xi \mathcal{P}_\sigma[\xi] \delta_F \left[\dot{x}(t) + f(x(t)) - \sum_{j=1}^k J_j g(x(t), x_j(t)) - \xi(t) \right]. \quad (51)$$

Once we determine $\mathcal{Q}[x]$ from the solutions of the above equation, the path-probability $\mathcal{P}[x]$ follows from

$$\mathcal{P}[x] = \sum_{k,\ell=0}^{\infty} p_{k,\ell} \int \left(\prod_{j=1}^k Dx_j \mathcal{Q}[x_j] \right) \int \left(\prod_{j=1}^k dJ_j p_J(J_j) \right) \int D\xi \mathcal{P}_\sigma[\xi] \delta_F \left[\dot{x}(t) + f(x(t)) - \sum_{j=1}^k J_j g(x(t), x_j(t)) - \xi(t) \right]. \quad (52)$$

Equations (51) and (52) make up the main analytic result of this work. Interestingly, these equations are formally similar to those determining the eigenvector distribution of sparse directed networks [6, 7]. When the degrees K_i and L_i are statistically independent at any node i , the joint degree distribution factorizes, $p_{k,\ell} = p_{\text{in},k} p_{\text{out},\ell}$, and the solution of the model reduces to a single self-consistent equation for the path-probability:

$$\mathcal{P}[x] = \sum_{k=0}^{\infty} p_{\text{in},k} \int \left(\prod_{j=1}^k Dx_j \mathcal{P}[x_j] \right) \int \left(\prod_{j=1}^k dJ_j p_J(J_j) \right) \int D\xi \mathcal{P}_\sigma[\xi] \delta_F \left[\dot{x}(t) + f(x(t)) - \sum_{j=1}^k J_j g(x(t), x_j(t)) - \xi(t) \right]. \quad (53)$$

III. POPULATION DYNAMICS ALGORITHM

Here we explain how to generalize the population dynamics algorithm [1, 3, 8] to efficiently solve the self-consistent Eq. (53) for the path-probability describing dynamical processes on directed random networks with uncorrelated degrees (K_i, L_i) . The algorithm is based on the introduction of a large population of stochastic trajectories that parametrize the path-probability $\mathcal{P}[x]$. These dynamical paths are then consistently updated according to Eq. (53). Informally speaking, the population dynamics algorithm is a Monte-Carlo approach to solve self-consistent distributional equations by iteration, analogous to finding the roots of a transcendental fixed-point equation by direct iteration. In the standard version of the algorithm [1–3], the probability density under study characterizes the statistics of a single random variable, while here one has to generalize the algorithm to deal with the probability density of functions of time. Each stochastic trajectory is constrained to the differential equation imposed by the Dirac functional- δ_F in Eq. (53). The most important aspect of the algorithm in the present case is that a single update refers to an *entire* stochastic trajectory, rather than to a single variable representing a particular instant of time. Apart from this nuance, the core of the algorithm remains conceptually the same as in standard applications.

Below we present a detailed account of the population dynamics algorithm in the absence of Gaussian noise ($\sigma = 0$). For concreteness, we detail all steps of the algorithm on the neural network model of [4], where $f(x) = x$ and

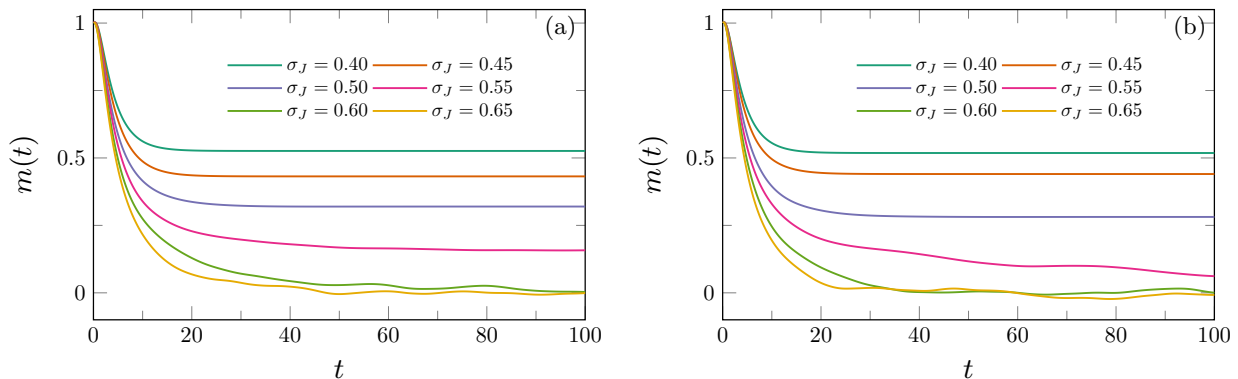


FIG. 1. Dynamics of $m(t)$ for the NN model (see table I in the main text) on directed random networks with a Poisson indegree distribution with mean degree $c = 4$. The random coupling strengths are sampled from a distribution p_J with mean $\mu_J = 1/3$ and standard deviation σ_J . The results are derived from the solutions of Eq. (54) using the population dynamics algorithm with 5×10^5 paths. The panels illustrate the universal transition between the nontrivial fixed-point phase II and the chaotic phase III. (a) Gaussian distribution p_J . (b) Uniform distribution p_J .

$g(x, x') = \tanh(x')$. In this particular setting, Eq. (53) assumes the form

$$\mathcal{P}[x] = \sum_{k=0}^{\infty} p_{\text{in},k} \int \left(\prod_{j=1}^k Dx_j \mathcal{P}[x_j] \right) \int \left(\prod_{j=1}^k dJ_j p_J(J_j) \right) \delta_F \left[\dot{x}(t) + x(t) - h_k[\{J_j, x_j(t)\}] \right], \quad (54)$$

where we defined the time-dependent local field

$$h_k[\{J_j, x_j(t)\}] = \sum_{j=1}^k J_j \tanh(x_j(t)). \quad (55)$$

The extension of the population dynamics algorithm to other models and to nonzero Gaussian noise ($\sigma > 0$) is straightforward.

In figure 1, we present results for the dynamics of $m(t)$ across the transition between the nontrivial fixed-point phase II and the chaotic phase III (see figure 2 in the main text). When the variance σ_J^2 of the coupling strengths is large enough, the fixed-point solution $m = m(t) > 0$ becomes unstable and the macroscopic parameter $m(t)$ displays aperiodic oscillations around zero. This transition to the chaotic regime occurs, for $c = 4$ and $\mu_J = 1/3$, at some critical value in the interval $\sigma_J \in (0.55, 0.60)$, which is consistent with the value $\sigma_J = 1/\sqrt{3}$ obtained from equation $c = 1 + \sigma_J^2/\mu_J^2$ (see the dashed line in figure 2 of the main text). The latter expression identifies the universal gap-gapless transition in the spectrum of directed random networks [9]: for $\sigma_J^2 < (c-1)\mu_J^2$ (phase II), the leading eigenvalue λ_1 of the adjacency matrix is separated from the second leading eigenvalue λ_2 by a finite gap $|\lambda_1 - \lambda_2| > 0$, while for $\sigma_J^2 \geq (c-1)\mu_J^2$ (phase III) we get $|\lambda_1 - \lambda_2| = 0$. The results in figure 1 lead us to conjecture that the transition between phases II and III coincides with the vanishing of the gap.

Algorithm 1 Population dynamics algorithm to solve Eq. (54) and determine the macroscopic observables $m(t)$ and $q(t)$ as a function of time. For simplicity, we illustrate the algorithm in conjunction with the Euler method for solving differential equations.

Inputs: indegree distribution $p_{in,k}$, distribution p_J of coupling strengths, population size M , total number N_{iter} of single-trajectory updates, total number T of points in a discretized path, and time increment ϵ of the Euler method.

Outputs: macroscopic observables $m(t)$ and $q(t)$ at time t .

Set the indegree distribution $p_{in,k}$ and the distribution $p_J(J)$ of coupling strengths.

Set the matrix $x[t][i]$ ($i = 1, \dots, M$ and $t = 0, \dots, T$) that stores the state variables along the i th dynamical trajectory.

Initialize all matrix elements $x[t][i]$. The entries $\{x[0][i]\}_{i=1, \dots, M}$ fix the initial condition.

repeat

 Select a single element i uniformly at random from the indexes $1, \dots, M$.

 Draw a non-negative random integer k from the distribution $p_{in,k}$.

 Create a set ∂_k with k elements selected uniformly at random from the indexes $1, \dots, M$.

 Create a set with elements J_1, \dots, J_k sampled from the distribution $p_J(J)$.

 Update the local fields $h[1][i], \dots, h[T][i]$ along the trajectory i : $h[t][i] \leftarrow \sum_{j \in \partial_k} J_j \tanh(x[t-1][i])$ \triangleright Eq. (55)

 Update the i th trajectory $x[1][i], \dots, x[T][i]$ (Euler method): $x[t][i] \leftarrow x[t-1][i] + \epsilon(-x[t-1][i] + h[t][i])$

until step number $< N_{iter}$

return $m(t) \leftarrow \frac{1}{M} \sum_{i=1}^M x[t][i]$ and $q(t) \leftarrow \frac{1}{M} \sum_{i=1}^M (x[t][i])^2$

IV. THE HIGH-CONNECTIVITY LIMIT

An important question is to understand whether the solution of the present class of models converges to the well-known results for fully-connected models as $c \rightarrow \infty$ [4, 10, 11]. Put differently, we aim to probe the universality of fully-connected models in the present context. In a series of recent works [12, 13], it has been shown that spin models on random networks do not converge to their fully-connected counterparts as $c \rightarrow \infty$, but the final solution is determined by the empirical distribution of the degrees rescaled by their mean. In the present context, we also expect that the universality of fully-connected architectures breaks down as $c \rightarrow \infty$, and the path-probability $\mathcal{P}[x]$ retains information about degree fluctuations even in the high-connectivity limit. In this subsection, we explain how to take the limit $c \rightarrow \infty$ of Eq. (53) and obtain the form of $\mathcal{P}[x]$ in the high-connectivity limit. We derive generic analytic results, valid for arbitrary functions $f(x)$ and $g(x, x')$ (see Eq. (1) and table I in the main text), which encapsulates a broad range of important models in the study of complex systems.

By using the functional Fourier transform of the Dirac- δ_F in Eq. (53), we can integrate over the Gaussian noise $\xi(t)$ and obtain the formal expression

$$\mathcal{P}[x] = \int D\hat{x} e^{i \int dt \hat{x}(t)[\dot{x}(t) + f(x(t))] - \frac{\sigma^2}{2} \int dt \hat{x}^2(t)} \sum_{k=0}^{\infty} p_{in,k} \exp \left[k \ln \left(\int Dx' \mathcal{P}[x'] \left\langle e^{-iJ \int dt \hat{x}(t)g(x(t), x'(t))} \right\rangle_J \right) \right], \quad (56)$$

where $\langle \dots \rangle_J$ denotes the average over J with respect to its distribution p_J . As we are interested in the high-connectivity limit $c \rightarrow \infty$, it is sensible to rescale the coupling strengths with c in such a way that $\mathcal{P}[x]$ converges to a finite limit. Therefore, we assume that the first two moments of J are given by

$$\int_{-\infty}^{\infty} dJ J p_J(J) = \frac{\mu_J}{c} \quad \text{and} \quad \int_{-\infty}^{\infty} dJ J^2 p_J(J) = \frac{\gamma_J^2}{c}, \quad (57)$$

while higher-order moments of J decay faster than $1/c$. For large c , we can expand the logarithm in Eq. (56) up to $\mathcal{O}(1/c)$, obtaining

$$\begin{aligned} \ln \left(\int Dx' \mathcal{P}[x'] \left\langle e^{-iJ \int dt \hat{x}(t)g(x(t), x'(t))} \right\rangle_J \right) &= -\frac{i\mu_J}{c} \int dt \hat{x}(t) \int Dx' \mathcal{P}[x'] g(x(t), x'(t)) \\ &\quad - \frac{\gamma_J^2}{2c} \int dt dt' \hat{x}(t)\hat{x}(t') \int Dx' \mathcal{P}[x'] g(x(t), x'(t)) g(x(t'), x'(t')). \end{aligned} \quad (58)$$

The above expression depends on functional averages of one-time and two-time quantities with respect to the path-probability $\mathcal{P}[x']$. By defining the conditional macroscopic parameters

$$M(t|x(t)) = \int Dx' \mathcal{P}[x'] g(x(t), x'(t)) \quad \text{and} \quad C(t, t'|x(t), x(t')) = \int Dx' \mathcal{P}[x'] g(x(t), x'(t)) g(x(t'), x'(t')), \quad (59)$$

the logarithmic contribution can be written in the compact form

$$\ln \left(\int Dx' \mathcal{P}[x'] \left\langle e^{-iJ \int dt \hat{x}(t) g(x(t), x'(t))} \right\rangle_J \right) = -\frac{i\mu_J}{c} \int dt \hat{x}(t) M(t|x(t)) - \frac{\gamma_J^2}{2c} \int dt dt' \hat{x}(t) \hat{x}(t') C(t, t'|x(t), x(t')). \quad (60)$$

Inserting the above expression back into Eq. (56) and introducing the distribution of rescaled indegrees [12, 13],

$$\nu_{\text{in}}(\kappa) = \lim_{c \rightarrow \infty} \sum_{k=0}^{\infty} p_{\text{in},k} \delta \left(\kappa - \frac{k}{c} \right), \quad (61)$$

we get

$$\begin{aligned} \mathcal{P}[x] &= \int_0^{\infty} d\kappa \nu_{\text{in}}(\kappa) \int D\hat{x} \exp \left(i \int dt \hat{x}(t) [\dot{x}(t) + f(x(t)) - \mu_J \kappa M(t|x(t))] \right) \\ &\quad \times \exp \left(-\frac{1}{2} \int dt dt' \hat{x}(t) \hat{x}(t') [\sigma^2 \delta(t-t') + \gamma_J^2 \kappa C(t, t'|x(t), x(t'))] \right). \end{aligned} \quad (62)$$

Finally, we can define the conditional covariance matrix

$$\Delta_{\kappa}(t, t'|x(t), x(t')) = \sigma^2 \delta(t-t') + \gamma_J^2 \kappa C(t, t'|x(t), x(t')) \quad (63)$$

and rewrite Eq. (62) as follows

$$\mathcal{P}[x] = \int_0^{\infty} d\kappa \nu_{\text{in}}(\kappa) \int D\omega \mathcal{P}[\omega|\kappa] \delta_F \left[\dot{x}(t) + f(x(t)) - \mu_J \kappa M(t|x(t)) - \omega(t) \right], \quad (64)$$

where $\omega(t)$ is a temporal correlated noise with the functional distribution

$$\mathcal{P}[\omega|\kappa] = \frac{1}{\mathcal{N}_{\omega}} \exp \left(-\frac{1}{2} \int dt dt' \omega(t) \omega(t') \Delta_{\kappa}^{-1}(t, t'|x(t), x(t')) \right), \quad (65)$$

conditioned to a fixed rescaled degree κ . The factor \mathcal{N}_{ω} ensures that $\int D\omega \mathcal{P}[\omega|\kappa] = 1$.

Equation (64) gives the analytic form of the path-probability density in the limit $c \rightarrow \infty$. Clearly, $\mathcal{P}[x]$ is determined by the distribution $\nu_{\text{in}}(\kappa)$ of rescaled indegrees, which means that the effective dynamics retains information about the network degree fluctuations even in the limit $c \rightarrow \infty$. Put differently, Eq. (64) demonstrates that the effective dynamics of fully-connected networks is not universal, in the sense that models on sparse networks do not generally flow to their fully-connected counterparts as the mean degree c diverges. This (perhaps surprising) nonuniversal character is not exclusive to the continuous-time dynamics of complex systems, but it has been previously identified in the context of Ising spin models [12, 13] and random matrix theory [14, 15].

For homogeneous networks, in which the indegree distribution $p_{\text{in},k}$ is such that $\nu_{\text{in}}(\kappa) = \delta(\kappa - 1)$, we expect to recover previous analytic results for the effective dynamics of models on fully-connected networks. Typical examples of homogeneous networks are regular networks ($p_{\text{in},k} = \delta_{k,c}$) and networks with Poisson indegrees ($p_{\text{in},k} = c^k e^{-c}/k!$). In both cases, it is straightforward to check from Eq. (61) that $\nu_{\text{in}}(\kappa) = \delta(\kappa - 1)$.

Finally, let us explicitly recover previous analytic results in the case of homogeneous networks. Here we focus on two particular examples: the Lotka-Volterra (LV) model and the neural network (NN) model of [4]. For the NN model, we have $f(x) = x$ and $g(x, x') = \tanh(x')$ (see table I in the main text), and Eq. (64) assumes the form

$$\mathcal{P}_{\text{NN}}[x] = \int_0^{\infty} d\kappa \nu_{\text{in}}(\kappa) \int D\omega \mathcal{P}[\omega|\kappa] \delta_F \left[\dot{x}(t) + x(t) - \mu_J \kappa M(t) - \omega(t) \right], \quad (66)$$

where the covariance of $\omega(t)$ reads

$$\Delta_{\kappa}(t, t') = \sigma^2 \delta(t-t') + \gamma_J^2 \kappa C(t, t'), \quad (67)$$

with

$$M(t) = \int Dx' \mathcal{P}[x'] \tanh(x'(t)) \quad \text{and} \quad C(t, t') = \int Dx' \mathcal{P}[x'] \tanh(x'(t)) \tanh(x'(t')). \quad (68)$$

Equations (66-68) enable to study the role of indegree heterogeneities in the high-connectivity limit of the NN model. As expected, when $\nu_{\text{in}}(\kappa) = \delta(\kappa - 1)$, Eqs. (66-68) reduce to the equations describing the effective dynamics of fully-connected models with independent Gaussian interactions [4, 5, 16]. For the LV model, we have that $f(x) = x(x - 1)$ and $g(x, x') = xx'$, and the path-probability becomes

$$\mathcal{P}_{\text{LV}}[x] = \int_0^\infty d\kappa \nu_{\text{in}}(\kappa) \int D\omega \mathcal{P}[\omega|\kappa] \delta_F \left[\dot{x}(t) + x(t)(x(t) - 1) - \mu_J \kappa x(t)M(t) - \omega(t) \right], \quad (69)$$

where the covariance of $\omega(t)$ reads

$$\Delta_\kappa(t, t'|x(t), x(t')) = \sigma^2 \delta(t - t') + \gamma_J^2 \kappa x(t)x(t')C(t, t'), \quad (70)$$

with

$$M(t) = \int Dx' \mathcal{P}[x'] x'(t) \quad \text{and} \quad C(t, t') = \int Dx' \mathcal{P}[x'] x'(t) x'(t'). \quad (71)$$

When $\nu_{\text{in}}(\kappa) = \delta(\kappa - 1)$ and $\sigma = 0$, Eqs. (69-71) yield the effective dynamics of the corresponding fully-connected Lotka-Volterra model with independent Gaussian couplings [17]. The results obtained here for the Lotka-Volterra model in the limit $c \rightarrow \infty$ are closely related to recent works [18, 19].

-
- [1] M Mézard and G Parisi, “The bethe lattice spin glass revisited,” *Eur. Phys. J. B* **20**, 217–233 (2001).
 - [2] M Mézard and G Parisi, “The cavity method at zero temperature,” *J. Stat. Phys.* **111**, 1–34 (2003).
 - [3] Fernando Lucas Metz, Izaak Neri, and Tim Rogers, “Spectral theory of sparse non-hermitian random matrices,” *Journal of Physics A: Mathematical and Theoretical* **52**, 434003 (2019).
 - [4] H. Sompolinsky, A. Crisanti, and H. J. Sommers, “Chaos in random neural networks,” *Phys. Rev. Lett.* **61**, 259–262 (1988).
 - [5] A. Crisanti and H. Sompolinsky, “Path integral approach to random neural networks,” *Phys. Rev. E* **98**, 062120 (2018).
 - [6] Izaak Neri and Fernando Lucas Metz, “Linear stability analysis of large dynamical systems on random directed graphs,” *Phys. Rev. Res.* **2**, 033313 (2020).
 - [7] Fernando Lucas Metz and Izaak Neri, “Localization and universality of eigenvectors in directed random graphs,” *Phys. Rev. Lett.* **126**, 040604 (2021).
 - [8] Reimer Kühn, “Spectra of sparse random matrices,” *Journal of Physics A: Mathematical and Theoretical* **41**, 295002 (2008).
 - [9] Izaak Neri and Fernando Lucas Metz, “Eigenvalue outliers of non-hermitian random matrices with a local tree structure,” *Phys. Rev. Lett.* **117**, 224101 (2016).
 - [10] Guy Bunin, “Ecological communities with lotka-volterra dynamics,” *Phys. Rev. E* **95**, 042414 (2017).
 - [11] Carles Martorell, Rubén Calvo, Alessia Annibale, and Miguel A. Muñoz, “Dynamically selected steady states and criticality in non-reciprocal networks,” *Chaos, Solitons and Fractals* **182**, 114809 (2024).
 - [12] Fernando L Metz and Thomas Peron, “Mean-field theory of vector spin models on networks with arbitrary degree distributions,” *Journal of Physics: Complexity* **3**, 015008 (2022).
 - [13] Leonardo S. Ferreira and Fernando L. Metz, “Nonequilibrium dynamics of the ising model on heterogeneous networks with an arbitrary distribution of threshold noise,” *Phys. Rev. E* **107**, 034127 (2023).
 - [14] Fernando L. Metz and Jeferson D. Silva, “Spectral density of dense random networks and the breakdown of the wigner semicircle law,” *Phys. Rev. Res.* **2**, 043116 (2020).
 - [15] Jeferson D Silva and Fernando L Metz, “Analytic solution of the resolvent equations for heterogeneous random graphs: spectral and localization properties,” *Journal of Physics: Complexity* **3**, 045012 (2022).
 - [16] Jannis Schuecker, Sven Goedeke, and Moritz Helias, “Optimal sequence memory in driven random networks,” *Phys. Rev. X* **8**, 041029 (2018).
 - [17] Tobias Galla, “Dynamically evolved community size and stability of random lotka-volterra ecosystems(a),” *Europhysics Letters* **123**, 48004 (2018).
 - [18] Jong Il Park, Deok-Sun Lee, Sang Hoon Lee, and Hye Jin Park, “Incorporating heterogeneous interactions for ecological biodiversity,” (2024), arXiv:2403.15730 [physics.bio-ph].
 - [19] Fabián Aguirre-López, “Heterogeneous mean-field analysis of the generalized lotka-volterra model on a network,” (2024), arXiv:2404.11164 [cond-mat.dis-nn].